

Ab initio charge form factors and radii of light isoscalar nuclei: Role of the two-body charge density

Xiang-Xiang Sun^{1,*}, Vadim Baru^{2,†}, Arseniy A. Filin^{2,‡}, Evgeny Epelbaum^{2,§},
Hermann Krebs^{2,¶}, Ulf-G. Meißner^{3,1,4,5,**} and Andreas Nogga^{1,5,||}

¹*Institute for Advanced Simulation (IAS-4), Forschungszentrum Jülich, D-52425 Jülich, Germany*

²*Institut für Theoretische Physik II, Ruhr-Universität Bochum, D-44780 Bochum, Germany*

³*Helmholtz-Institut für Strahlen- und Kernphysik and Bethe Center for Theoretical Physics,
Universität Bonn, D-53115 Bonn, Germany*

⁴*Peng Huanwu Collaborative Center for Research and Education,*

International Institute for Interdisciplinary and Frontiers, Beihang University, Beijing 100191, China

⁵*CASA, Forschungszentrum Jülich, 52425 Jülich, Germany*

(Dated: January 15, 2026)

We make *ab initio* predictions of charge form factors (FFs) and radii for the isoscalar nuclei ^6Li and ^8Be using the Jacobi-coordinate No-Core Shell Model. The calculations employ chiral semilocal momentum-space regularized two- and three-nucleon interactions, together with consistently regularized one- and two-nucleon electromagnetic charge operators. With the short-range charge density fixed to the ^4He charge radius, the predicted FFs and the ^6Li radius show good agreement with available experimental data. We find that two-nucleon charge density contributions are essential for describing the FFs, particularly at intermediate and large momentum transfers. Although their influence on the charge radii is limited, these contributions remain crucial for attaining accurate predictions. The present results highlight the importance of two-nucleon charge operators in addressing the long-standing underestimation of nuclear charge radii in *ab initio* calculations based on modern chiral interactions.

Introduction—Electromagnetic probes offer a uniquely incisive tool for investigating nuclear structure [1–4]. The weak nature of the electromagnetic coupling (characterized by the fine-structure constant) simplifies the reaction mechanism, establishing a clear and direct link between experimentally measured cross sections and computed nuclear structure properties [1,5]. Elastic electron scattering experiments, in particular, yield crucial information on a nucleus’s charge and magnetic form factors (FFs), which are functions of the momentum transfer squared (Q^2), and reflect the spatial distributions of charge and magnetization within the nucleus. The charge radius, derived from the charge form factor at zero momentum transfer, serves as a fundamental measure of the spatial extent of the nuclear charge distribution. Recent breakthroughs in experimental techniques, including ultra-high precision atomic spectroscopy measurements, have provided charge radii and magnetic moments with unprecedented accuracy [6–9]. These high-precision data from various advanced experimental techniques provide stringent tests for theoretical models of nuclear forces and currents, as well as for nuclear structure [10–17]. The quest for a profound understanding of the nuclear structure and dynamics of atomic nuclei stands as a central, long-standing challenge in nuclear physics [10,12,18–26].

Atomic nuclei are complex many-body systems composed of protons and neutrons, bound together by the strong nucleon-nucleon interaction. Chiral Effective Field Theory (χ EFT) rooted in QCD serves as a robust framework for describing nuclear forces and currents [5,27–32]. This approach enables systematic improvements in theoretical precision and allows for quantifying

uncertainties stemming from neglected higher-order contributions. χ EFT is crucial to methodically explore the internal structure and dynamics of atomic nuclei through electromagnetic observables. A key advantage of χ EFT lies in its ability to provide electromagnetic current operators that are consistent with nuclear forces [2,4,5,33–38]. To achieve reliable predictions, both nuclear potentials and current operators must be derived and regularized within the same framework, while inconsistent regularization, for example, can lead to violations of chiral symmetry [5]. The use of consistent regularization is essential for obtaining precise results and for validating the theoretical framework by, e.g., demonstrating that observables are independent of unphysical effects like unitary ambiguities [5,39]. Recent developments in χ EFT have focused on implementing consistent regularization methods for both nuclear forces and currents. In particular, a rigorous regularization scheme in χ EFT, which preserves chiral and gauge symmetries, has been developed in [40,41] using the chiral gradient flow. This approach is currently being applied to derive the subleading three-nucleon forces and loop contributions to the nuclear charge and current operators. The isoscalar contributions to the two-body charge density needed in this study, however, involve only tree-level contributions, whose regularized expressions can be found in [39].

Precise calculations of charge FFs and radii have been achieved for the deuteron using advanced high-order nuclear interactions from χ EFT with consistently regularized densities and current operators, demonstrating that two-body charge operators play an important role [39,42]. Preliminary results from a combined analysis of light nu-

clei with $A \leq 4$ suggest similar conclusions [43]. However, the role of two-body operators in the charge FFs and radii of heavier nuclei are still unclear. As an important step towards the application to complex nuclei, this work aims to determine the charge FFs and radii for p -shell nuclei ^6Li and ^8Be , including two-nucleon currents and reveal their importance with increasing system size.

Theoretical framework—The nuclear many-body wave functions are obtained by using the Jacobi-NCSM [44–48] with the SRG evolved semilocal momentum-space-regularized (SMS) NN potential at the order N^4LO^+ with momentum cutoffs $\Lambda_N = 450$ and 500 MeV [49], together with a consistent 3N potential at N^2LO (SMS $\text{N}^4\text{LO}^+ + \text{N}^2\text{LO}$), which provide a nearly perfect description of the binding energies of light nuclei [22,23]. Along with these SMS interactions, the consistently regularized charge density has been developed for the isoscalar channel [5,39,42] and the involved low-energy coupling constants (LECs) can be determined from the light-nuclei data as described below.

The charge FFs of the ground state are obtained by

$$\begin{aligned} \langle JM' | \hat{O}(\vec{q}, \vec{k}) | JM \rangle \\ = \langle JM' | \begin{pmatrix} A \\ 1 \end{pmatrix} \hat{O}_{1b}(\vec{q}, \vec{k}) + \begin{pmatrix} A \\ 2 \end{pmatrix} \hat{O}_{2b}(\vec{q}, \vec{k}) | JM \rangle, \end{aligned} \quad (1)$$

where \vec{k} is the incident momentum of the probe, \vec{q} is the momentum transfer, J is the spin of the ground state and M' and M are the projections of J . The charge FFs of $A \geq 4$ isoscalar nuclei are calculated using the transition-density formalism [50]. In this way, the matrix of one-body (\hat{O}_{1b}) and two-body (\hat{O}_{2b}) charge density operators in different partial waves calculated using a numerical partial wave decomposition based on Ref. [51], are convoluted with one- and two-body transition densities encoding the nuclear many-body wave functions. The densities are constructed based on the J-NCSM wave function and available online at [52]. More details can be found in Sec. A in [53]. The nucleon FFs in the charge density operators are taken from the dispersive analysis of Ref. [54], which yields a proton charge radius consistent with the CODATA-2022 value.

The charge radius for an isoscalar nucleus is composed of the contribution of the matter radius, the proton and neutron charge radii, Darwin-Foldy (DF), spin-orbit (SO), two-body contact, and the one-pion-exchange (1π) terms

$$R_c^2 = r_m^2 + r_p^2 + r_n^2 + r_{\text{DF}}^2 + r_{\text{SO}}^2 + r_{1\pi}^2 + r_{\text{Cont}}^2, \quad (2)$$

where the proton charge radius is $r_p = 0.84075(64)$ fm from the CODATA-2022 [55] and the mean-squared neutron charge radius $r_n^2 = -0.105^{+0.005}_{-0.006}$ fm 2 is taken from Refs. [39,42].

Determination of the LECs—For the two-body charge densities, the 1π term has no free parameters, while the

isoscalar short-range part depends on three LECs. The deuteron charge and quadrupole FFs were used in [39,42] to determine the two LECs in the isospin-zero-to-isospin-zero channel for the SMS interactions we employ here. In this work, we fix the remaining LEC in the isospin-one-to-isospin-one channel by fitting it to the experimental value of the ^4He charge radius, see Sec. B in the Supplemental Material [53] for details.

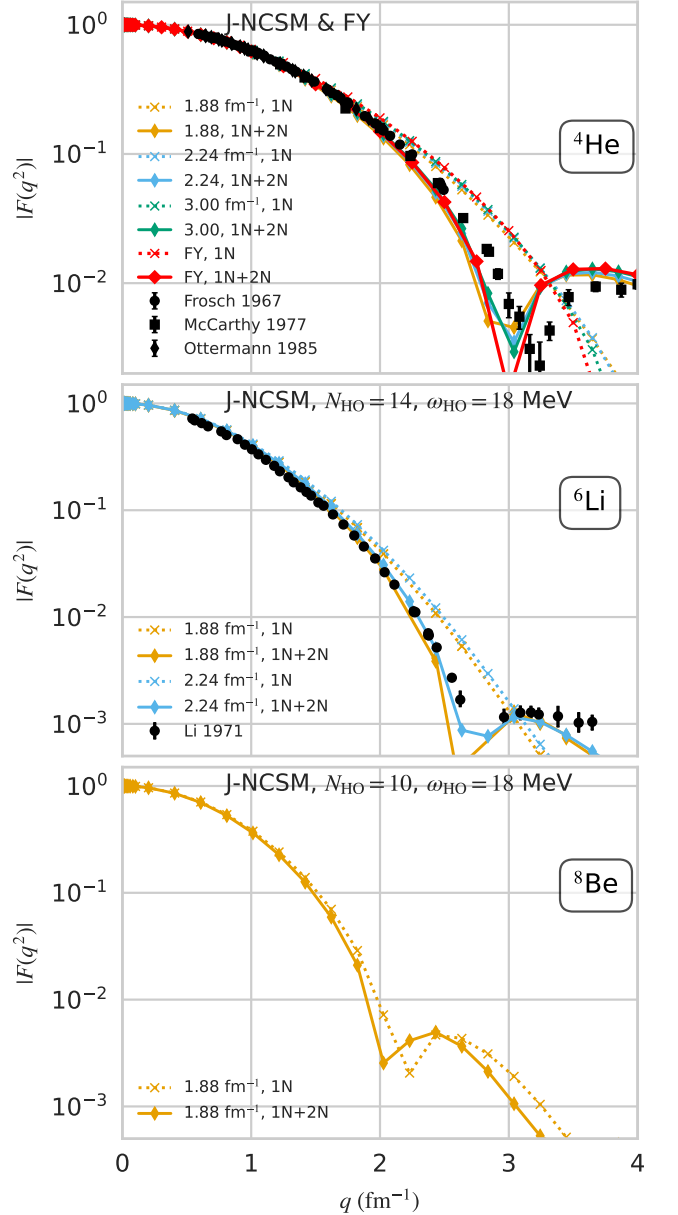


FIG. 1. Charge form factors for ^4He , ^6Li and ^8Be with SMS interaction $\Lambda_N = 450$ MeV. The experimental data of ^4He are taken from Frosch 1967 [56], McCarthy 1977 [57], Ottermann 1985 [58]. Data for ^6Li is from Li 1971 [59].

Charge form factors and radii—The charge FFs for ^4He , ^6Li and ^8Be , calculated using the SMS interaction with $\Lambda_N = 450$ MeV and taking into account the

one-body (1N) and the combined one- and two-body (1N+2N) contributions to the charge FFs are shown in Fig. 1. In the J-NCSM calculations, we use the SRG evolved SMS interactions and the corresponding one-body density matrix. For the two-body densities, we apply a unitary transformation to the J-NCSM wave function to eliminate the influence from the SRG [60]. The inclusion of two-body currents significantly affects the form factor in the intermediate- and large- q regions, shifting the diffraction minimum to lower values of q , thereby improving the agreement with experimental data for ${}^4\text{He}$ and ${}^6\text{Li}$.

For the benchmark nucleus ${}^4\text{He}$, J-NCSM calculations yield converged results with a large model space, which can be compared with charge FFs using the density matrix from the Faddeev-Yakubovsky (FY) method with the bare SMS interactions. From Fig. 1, it is clear that with the increase of the SRG flow parameter λ [61] from 1.88 fm^{-1} to 3.00 fm^{-1} , the results get closer to the FY calculations. The tiny differences mainly originate from the neglected SRG transformation on the one-body density (see the deviations of the 1N part above 3.5 fm^{-1}) and the center-of-mass motion between the two-body pair and the remaining cluster. In result, the FFs from J-NCSM are slightly smaller than those from FY when momentum transfers are smaller than the diffraction minimum (around 3.2 fm^{-1}).

For ${}^6\text{Li}$, we calculate its FFs with different basis properties: the harmonic oscillator (HO) frequency ω and the maximal HO excitation N_{HO} (see Supplemental Material [53]). The dependence on the model space parameters turns out to be insignificant. Therefore, in Fig. 1, we only show the results using $\omega_{\text{HO}} = 18 \text{ MeV}$ and $N_{\text{HO}} = 14$ with two SRG flow parameters, for which the binding energy of ${}^6\text{Li}$ is well reproduced. The calculated FFs are consistent with the data when the 2N contributions are included, with only a slight underestimation observed in the region $2 < q < 3 \text{ fm}^{-1}$. To further investigate the relative importance of the 2N charge density contributions, we also consider the unbound ${}^8\text{Be}$ nucleus. In this case, direct comparison to experimental data is not possible, as no data are available. However, comparing the 1N and 2N charge density contributions indicates that their relative size stabilizes as the system size increases. Additionally, we also performed calculations with the SMS interaction $\Lambda_N = 500 \text{ MeV}$ and the same conclusions are obtained.

The individual contributions to the charge radius from the point-proton radius r_m , DF and SO terms $\Delta R_{\text{DF+SO}}$, and 2N contact and 1π operators $\Delta R_{\text{Cont+1}\pi}$ are listed in Table I and shown in Fig. 2. As mentioned before, the extracted r_m does not account for the SRG effects when using the one-body density matrix corresponding to the SRG-evolved interaction. To evaluate this, we directly calculate $\langle \hat{r}^2 \rangle$ using the SRG evolved two-body density at zero momentum (see Ref. [65] and Sec. D in t[53] for

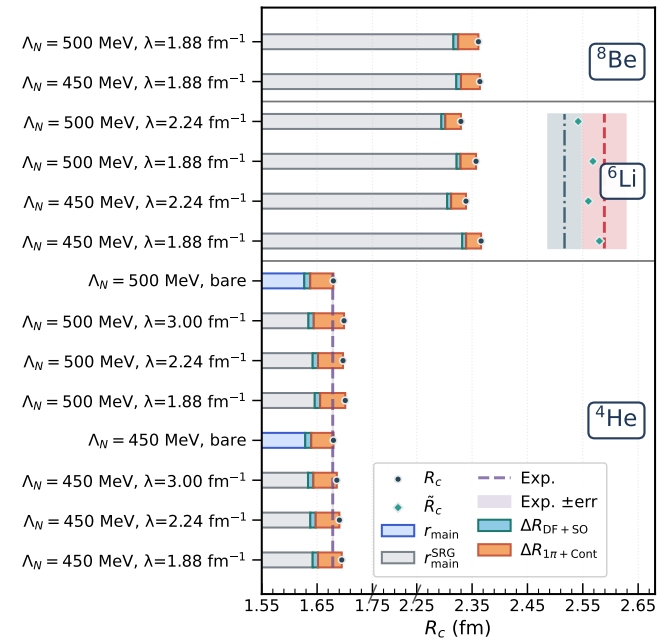


FIG. 2. Charge radii for ${}^4\text{He}$, ${}^6\text{Li}$ and ${}^8\text{Be}$ using the SMS interactions with $\Lambda_N = 450$ and 500 MeV corresponding to the result in Table I. The experimental data are indicated by the vertical lines with error bands. r_{main} (FY) is obtained from the matter radius r_m , while $r_{\text{main}}^{\text{SRG}}$ (J-NCSM) is obtained from the SRG-evolved matter radius r_m^{SRG} ; both include the proton and neutron charge radius contributions.

details). The resulting values are denoted by r_m^{SRG} and include two-nucleon SRG-induced contributions to the radius operator. For ${}^4\text{He}$, the J-NCSM calculation yields converged radii and energies in good agreement with the FY approach with the bare interactions. We find that as the SRG flow parameter increases, the obtained radius decreases and approaches the FY results, which by construction coincide with the most recent measurement [8]. The contributions from 2N operators with the SMS interactions for cutoffs $\Lambda_N = 450$ and 500 MeV , about 0.04 fm , are almost insensitive to the SRG transformation, visibly larger than the residual SRG dependence and are crucial for an accurate description of the charge radius. Notably, the importance of 2N contributions is consistent with preliminary results from a combined analysis of light nuclei ($A \leq 4$), as reported in Ref. [43].

Our J-NCSM calculations for the ${}^6\text{Li}$ charge radius do not yield a fully converged value; however, we find that the contributions from 2N charge operators exhibit stable convergence with increasing N_{HO} for different λ , see Fig. S3 in the Ref. [53]. In particular, for a harmonic oscillator frequency of $\omega = 16$ or 18 MeV , the 2N part of the charge radius, $\Delta R_{\text{Cont+1}\pi}$, is almost converged with respect to N_{HO} . Therefore, we show the total charge radius and its decomposition into various operator contributions using this basis parameter set. Inclusion of

TABLE I. Charge radii of isoscalar nuclei ^4He , ^6Li , and ^8Be using SMS interactions with $\Lambda_N = 450$ MeV and 500 MeV. The contributions from the matter radius r_m , the DF and SO terms $\Delta R_{\text{DF+SO}}$, and two-body contact and one-pion-exchange operators $\Delta R_{\text{Cont+1}\pi}$, are shown. r_m^{SRG} labels the matter radius calculated by using SRG evolved two-body densities at the zero-momentum transfer and R_c is the corresponding charge radius. \tilde{R}_c denotes the charge radius including the tail correction of the SRG-evolved two-body relative density distribution. Available experimental data (Exp.) are also shown. The last column shows the extrapolated energies using the exponential function for the J-NCSM calculations in comparison with data from Ref. [62] and the FY calculations.

	λ (fm $^{-1}$)	r_m (fm)	r_m^{SRG} (fm)	$\Delta R_{\text{DF+SO}}$ (fm)	$\Delta R_{\text{Cont+1}\pi}$ (fm)	R_c (fm)	\tilde{R}_c (fm)	E_b (MeV)
^4He N $^4\text{LO}^+ + \text{N}^2\text{LO}$ ($\Lambda_N = 450$ MeV)								
1.880	1.4665	1.4467	0.0097	0.0432		1.6945	1.6945	28.32
2.236	1.4524	1.4419	0.0097	0.0428		1.6899	1.6899	28.24
3.000	1.4411	1.4372	0.0097	0.0421		1.6850	1.6850	28.22
bare, FY	1.4315		0.0096	0.0404			1.6782 ^a	28.32
N $^4\text{LO}^+ + \text{N}^2\text{LO}$ ($\Lambda_N = 500$ MeV)								
1.880	1.4691	1.4510	0.0098	0.0457		1.7008	1.7008	28.34
2.236	1.4559	1.4467	0.0098	0.0454		1.6967	1.6967	28.23
3.000	1.4429	1.4380	0.0097	0.0450		1.6886	1.6886	28.23
bare, FY	1.4295		0.0095	0.0422			1.6782 ^a	28.53
Exp.							1.67824(83) [8]	28.29 [62]
^6Li N $^4\text{LO}^+ + \text{N}^2\text{LO}$ ($\Lambda_N = 450$ MeV), $\omega_{\text{HO}} = 18$ MeV, $N_{\text{HO}} = 14$								
1.880	2.2094	2.1990	0.0072	0.0271		2.3658	2.5851	31.29
2.236	2.1758	2.1702	0.0072	0.0269		2.3388	2.5640	31.27
N $^4\text{LO}^+ + \text{N}^2\text{LO}$ ($\Lambda_N = 500$ MeV)								
1.880	2.1996	2.1883	0.0072	0.0283		2.3571	2.5653	31.44
2.236	2.1649	2.1590	0.0072	0.0281		2.3295	2.5384	31.47
Exp.							2.517(30) [63]	31.99 [62]
							2.589(39) [64]	
^8Be N $^4\text{LO}^+ + \text{N}^2\text{LO}$ ($\Lambda_N = 450$ MeV), $\omega_{\text{HO}} = 18$ MeV, $N_{\text{HO}} = 10$								
1.880	2.1952	2.1877	0.0074	0.0347		2.3633		55.21
N $^4\text{LO}^+ + \text{N}^2\text{LO}$ ($\Lambda_N = 500$ MeV), $\omega_{\text{HO}} = 18$ MeV, $N_{\text{HO}} = 10$								
1.880	2.1941	2.1821	0.0074	0.0372		2.3605		55.18
Exp.								56.50 [62]

^a Value fitted to the experimental data for the ^4He charge radius.

the 2N contributions increases the charge radius of ^6Li by approximately 0.03 fm for both SMS interactions considered. Notably, using SRG-evolved two-body densities to evaluate the 2N operators can partially mitigate the dependence on the SRG flow parameter. To further verify the influence of the 2N contribution for large mass number nuclei, we calculate the charge radius of ^8Be , although it is unbound with respect to the α emission and there is no available charge radius data. For ^8Be , the 2N contributions increase the charge radius by approximately 0.035 fm. It is remarkable that the size of the 2N contribution does neither scale with the number of 2N pairs nor with the number of α clusters in the nucleus. It seems that the contribution is, to a large extent, driven by short-distance currents getting contributions mainly from 4 nucleons in the s -shell. The α -d (α - α) cluster structure of ^6Li (^8Be) is not reflected in our explicit results of the 2N contributions. The importance of the

2N contributions is clearly shown in Fig. 2, where one finds that $\Delta R_{\text{Cont+1}\pi}$ is much larger than the DF and SO terms. Recently, the role of two-body charge operators has also been investigated via variational Monte Carlo [66,67], but using different chiral interactions. The increase of ^6Li and ^8Be charge radii from two-body contributions found in our work is slightly larger than that in Ref. [67].

The uncertainties in our calculations primarily originate from three sources: (a) the truncation of the J-NCSM model space and variation of the SRG flow parameter λ , (b) the chiral order of the nuclear interactions and the corresponding charge currents and densities, and (c) the LECs associated with the charge density operators. For the ^6Li charge radius, the truncation error of χEFT , estimated conservatively as a N ^2LO contribution to \tilde{R}_c , exceeds the spread arising from the variation of the cutoff Λ (see Table I), yet remains clearly smaller

than the experimental error. The spread obtained from varying the SRG flow parameter λ is comparable to this truncation estimate. The statistical uncertainty associated with the propagated uncertainties of the LECs is negligible compared to all types of uncertainties, as demonstrated in [53]. The basis space limitation in the radius calculations is treated following Ref. [65], where a tail correction to the r -space two-body relative densities yields converged results. We apply this method to ${}^6\text{Li}$, obtaining charge radii denoted as \tilde{R}_c in Table I, which are consistent with experimental measurements, see also Fig. 2. For ${}^4\text{He}$, J-NCSM provides converged radii and $R_c = \tilde{R}_c$.

Summary—Using high-order chiral SMS interactions and consistently regularized charge density operators, we study the charge form factors and radii of light isoscalar nuclei. We find that two-nucleon charge density contributions are much larger than those from DF and SO terms and are essential not only for describing the form factors at intermediate and large momentum transfers but also for achieving an accurate determination of the charge radius. While the present study focuses on light isoscalar systems, the framework developed here can be extended to include consistently regularized isovector two-nucleon charge density operators (under development), and applied to heavier nuclei through alternative *ab initio* approaches. Our results suggest that two-nucleon charge operators could provide important contribution toward resolving the long-standing underestimation of nuclear charge radii in *ab initio* calculations. Their inclusion reduces the discrepancy between theory and experiment and is therefore essential for achieving quantitatively reliable predictions.

X.X.S. appreciates helpful discussion with Shan-Gui Zhou. This work was supported in part by the European Research Council (ERC) under the European Union’s Horizon 2020 research and innovation programme (grant agreement No. 101018170 and No. 885150) as well as by the MKW NRW under the funding code NW21-024-A, and by the CAS President’s International Fellowship Initiative (PIFI) under Grant No. 2025PD0022. The numerical calculations were performed on JURECA of the Jülich Supercomputing Centre, Jülich, Germany.

arXiv:nucl-th/0111015.

- [3] S. Bacca and S. Pastore, *J. Phys. G* **41**, 123002 (2014), arXiv:1407.3490 [nucl-th].
- [4] L. E. Marcucci, F. Gross, M. T. Pena, M. Piarulli, R. Schiavilla, I. Sick, A. Stadler, J. W. Van Orden, and M. Viviani, *J. Phys. G* **43**, 023002 (2016), arXiv:1504.05063 [nucl-th].
- [5] H. Krebs, *Eur. Phys. J. A* **56**, 234 (2020), arXiv:2008.00974 [nucl-th].
- [6] K. Schuhmann *et al.* (CREMA), *Science* **388**, adj2610 (2025).
- [7] Y. van der Werf, K. Steinebach, R. Jannin, H. L. Bethlem, and K. S. E. Eikema, *Science* **388**, adj2462 (2025).
- [8] J. J. Krauth *et al.*, *Nature* **589**, 527 (2021).
- [9] R. Pohl *et al.* (CREMA), *Science* **353**, 669 (2016).
- [10] R. F. Garcia Ruiz *et al.*, *Nature Phys.* **12**, 594 (2016), arXiv:1602.07906 [nucl-ex].
- [11] C. Gorges *et al.*, *Phys. Rev. Lett.* **122**, 192502 (2019).
- [12] A. Koszorús *et al.*, *Nature Phys.* **17**, 439 (2021), [Erratum: *Nature Phys.* 17, 539 (2021)], arXiv:2012.01864 [nucl-ex].
- [13] X. F. Yang, S. J. Wang, S. G. Wilkins, and R. F. Garcia Ruiz, *Prog. Part. Nucl. Phys.* **129**, 104005 (2023), arXiv:2209.15228 [nucl-ex].
- [14] K. König *et al.*, *Phys. Rev. Lett.* **132**, 162502 (2024), [Erratum: *Phys. Rev. Lett.* 133, 059901 (2024)], arXiv:2309.02037 [nucl-ex].
- [15] J. Warbivek *et al.*, *Nature* **634**, 1075 (2024).
- [16] S. W. Bai *et al.*, *Phys. Rev. Lett.* **134**, 182501 (2025), arXiv:2504.12001 [nucl-ex].
- [17] F. P. Gustafsson *et al.*, *Phys. Rev. Lett.* **135**, 222501 (2025), arXiv:2504.17060 [nucl-ex].
- [18] H. Hergert, *Phys. Scripta* **92**, 023002 (2017), arXiv:1607.06882 [nucl-th].
- [19] M. L. Bissell *et al.*, *Phys. Rev. C* **93**, 064318 (2016).
- [20] V. Lapoux, V. Somà, C. Barbieri, H. Hergert, J. D. Holt, and S. R. Stroberg, *Phys. Rev. Lett.* **117**, 052501 (2016), arXiv:1605.07885 [nucl-ex].
- [21] S. Kaur *et al.*, *Phys. Rev. Lett.* **129**, 142502 (2022), arXiv:2209.00722 [nucl-ex].
- [22] P. Maris *et al.*, *Phys. Rev. C* **103**, 054001 (2021), arXiv:2012.12396 [nucl-th].
- [23] P. Maris *et al.* (LENPIC), *Phys. Rev. C* **106**, 064002 (2022), arXiv:2206.13303 [nucl-th].
- [24] P. Maris, H. Le, A. Nogga, R. Roth, and J. P. Vary, *Front. in Phys.* **11**, 1098262 (2023), arXiv:2305.19648 [nucl-th].
- [25] S. Elhatisari *et al.*, *Nature* **630**, 59 (2024), arXiv:2210.17488 [nucl-th].
- [26] Z. Ren, S. Elhatisari, and U.-G. Meißner, *Phys. Rev. Lett.* **135**, 152502 (2025), arXiv:2506.02597 [nucl-th].
- [27] E. Epelbaum, H.-W. Hammer, and U.-G. Meißner, *Rev. Mod. Phys.* **81**, 1773 (2009), arXiv:0811.1338 [nucl-th].
- [28] R. Machleidt and D. R. Entem, *Phys. Rept.* **503**, 1 (2011), arXiv:1105.2919 [nucl-th].
- [29] B. R. Barrett, P. Navratil, and J. P. Vary, *Prog. Part. Nucl. Phys.* **69**, 131 (2013).
- [30] K. Hebeler, J. D. Holt, J. Menendez, and A. Schwenk, *Ann. Rev. Nucl. Part. Sci.* **65**, 457 (2015), arXiv:1508.06893 [nucl-th].
- [31] H. Hergert, S. K. Bogner, T. D. Morris, A. Schwenk, and K. Tsukiyama, *Phys. Rept.* **621**, 165 (2016), arXiv:1512.06956 [nucl-th].
- [32] D. R. Phillips, *Ann. Rev. Nucl. Part. Sci.* **66**, 421 (2016).
- [33] S. Kolling, E. Epelbaum, H. Krebs, and U.-G. Meißner,

* x.sun@fz-juelich.de

† vadimb@tp2.rub.de

‡ arseniy.filin@ruhr-uni-bochum.de

§ evgeny.epelbaum@ruhr-uni-bochum.de

¶ hermann.krebs@rub.de

** meissner@hiskp.uni-bonn.de

†† a.nogga@fz-juelich.de

- [1] T. W. Donnelly and I. Sick, *Rev. Mod. Phys.* **56**, 461 (1984).
- [2] R. A. Gilman and F. Gross, *J. Phys. G* **28**, R37 (2002),

Phys. Rev. C **80**, 045502 (2009), arXiv:0907.3437 [nucl-th].

[34] S. Kolling, E. Epelbaum, H. Krebs, and U.-G. Meißner, Phys. Rev. C **84**, 054008 (2011), arXiv:1107.0602 [nucl-th].

[35] H. Krebs, E. Epelbaum, and U.-G. Meißner, Few Body Syst. **60**, 31 (2019), arXiv:1902.06839 [nucl-th].

[36] S. Pastore, R. Schiavilla, and J. L. Goity, Phys. Rev. C **78**, 064002 (2008), arXiv:0810.1941 [nucl-th].

[37] S. Pastore, L. Girlanda, R. Schiavilla, M. Viviani, and R. B. Wiringa, Phys. Rev. C **80**, 034004 (2009), arXiv:0906.1800 [nucl-th].

[38] S. Pastore, L. Girlanda, R. Schiavilla, and M. Viviani, Phys. Rev. C **84**, 024001 (2011), arXiv:1106.4539 [nucl-th].

[39] A. A. Filin, D. Möller, V. Baru, E. Epelbaum, H. Krebs, and P. Reinert, Phys. Rev. C **103**, 024313 (2021), arXiv:2009.08911 [nucl-th].

[40] H. Krebs and E. Epelbaum, Phys. Rev. C **110**, 044003 (2024), arXiv:2311.10893 [nucl-th].

[41] H. Krebs and E. Epelbaum, Phys. Rev. C **110**, 044004 (2024), arXiv:2312.13932 [nucl-th].

[42] A. A. Filin, V. Baru, E. Epelbaum, H. Krebs, D. Möller, and P. Reinert, Phys. Rev. Lett. **124**, 082501 (2020), arXiv:1911.04877 [nucl-th].

[43] A. Filin, V. Baru, E. Epelbaum, C. Körber, H. Krebs, D. Möller, A. Nogga, and P. Reinert, Talk at the Marciana 2025 Workshop on Lepton Interactions with Nucleons and Nuclei, Marciana Marina, Isola d'Elba, Italy (2025), unpublished.

[44] S. Liebig, U.-G. Meißner, and A. Nogga, Eur. Phys. J. A **52**, 103 (2016), arXiv:1510.06070 [nucl-th].

[45] H. Le, J. Haidenbauer, U.-G. Meißner, and A. Nogga, Eur. Phys. J. A **56**, 301 (2020), arXiv:2008.11565 [nucl-th].

[46] H. Le, J. Haidenbauer, U.-G. Meißner, and A. Nogga, Phys. Rev. C **107**, 024002 (2023), arXiv:2210.03387 [nucl-th].

[47] H. Le, J. Haidenbauer, U.-G. Meißner, and A. Nogga, Eur. Phys. J. A **57**, 339 (2021), arXiv:2109.06648 [nucl-th].

[48] H. Le, J. Haidenbauer, U.-G. Meißner, and A. Nogga, Eur. Phys. J. A **60**, 3 (2024), arXiv:2308.01756 [nucl-th].

[49] P. Reinert, H. Krebs, and E. Epelbaum, Eur. Phys. J. A **54**, 86 (2018), arXiv:1711.08821 [nucl-th].

[50] H. W. Grießhammer, J. A. McGovern, A. Nogga, and D. R. Phillips, Few Body Syst. **61**, 48 (2020), arXiv:2005.12207 [nucl-th].

[51] C. Körber, Numerical partial wave decomposition, <https://github.com/ckoerber/numpwd>.

[52] A. Nogga *et al.*, NUCDENS: A package to access nuclear densities, <https://jugit.fz-juelich.de/a.nogga/nucldensity>.

[53] See the supplement materials for details on the calculations of the charge form factors, the determination of the LEC M3, the statistical uncertainties of the charge radii, the matter radius, and the charge form factors of ${}^6\text{Li}$ and ${}^8\text{Be}$.

[54] Y.-H. Lin, H.-W. Hammer, and U.-G. Meißner, Phys. Rev. Lett. **128**, 052002 (2022), arXiv:2109.12961 [hep-ph].

[55] P. J. Mohr, D. B. Newell, B. N. Taylor, and E. Tiesinga, Rev. Mod. Phys. **97**, 025002 (2025), arXiv:2409.03787 [hep-ph].

[56] R. F. Frosch, J. S. McCarthy, R. E. Rand, and M. R. Yearian, Phys. Rev. **160**, 874 (1967).

[57] J. S. McCarthy, I. Sick, and R. R. Whitney, Phys. Rev. C **15**, 1396 (1977).

[58] C. R. Ottermann, G. Kobschall, K. Maurer, K. Rohrich, C. Schmitt, and V. H. Walther, Nucl. Phys. A **436**, 688 (1985).

[59] G. C. Li, I. Sick, R. R. Whitney, and M. R. Yearian, Nucl. Phys. A **162**, 583 (1971).

[60] X.-X. Sun, H. Le, U.-G. Meißner, and A. Nogga, (2025), arXiv:2512.15454 [nucl-th].

[61] λ is a scaled flow parameter with $\lambda = (s/m_N^2)^{-1/4}$ with the nucleon mass m_N . s is the flow parameter in the unit of fm^4 .

[62] M. Wang, W. J. Huang, F. G. Kondev, G. Audi, and S. Naimi, Chin. Phys. C **45**, 030003 (2021).

[63] I. Tanihata, H. Savajols, and R. Kanungo, Prog. Part. Nucl. Phys. **68**, 215 (2013).

[64] W. Nörterhäuser, T. Neff, R. Sanchez, and I. Sick, Phys. Rev. C **84**, 024307 (2011).

[65] X.-X. Sun, H. Le, U.-G. Meißner, and A. Nogga, Phys. Rev. C **112**, 024317 (2025), arXiv:2502.03989 [nucl-th].

[66] G. B. King, G. Chambers-Wall, A. Gnech, S. Pastore, M. Piarulli, and R. B. Wiringa, Phys. Rev. C **110**, 054325 (2024), arXiv:2408.16909 [nucl-th].

[67] G. B. King, G. Chambers-Wall, A. Gnech, S. Pastore, M. Piarulli, and R. B. Wiringa, Phys. Rev. C **112**, L041302 (2025), arXiv:2504.04201 [nucl-th].

SUPPLEMENTAL MATERIALS OF “*AB INITIO* CHARGE FORM FACTORS AND RADII OF LIGHT ISOSCALAR NUCLEI: ROLE OF THE TWO-BODY CHARGE DENSITY”

A. Calculation of charge form factors

The calculation of the charge form factor [cf. Eq. (1)] is performed by using the density matrix expansion method. The one-body charge operator \hat{O}_{1b} including the main contribution, the Darwin-Foldy (DF) and spin-orbit (SO) contributions is calculated by [50]

$$\langle M' | \hat{O}_{1b} | M \rangle = \sum_{K=0}^{K_{\max}=1} \sum_{\kappa=-K}^K \sum_{m_s, m'_s, m_\tau} \rho_{1b}^{M'M, m_\tau} (\vec{k}, \vec{q}) \times \hat{O}_{1b}(K\kappa; \vec{q}, \vec{k}; m_\tau; m_s m'_s), \quad (S1)$$

with the spherical expansion order K and κ , and the spin-projection m_s and isospin projection m_τ .

The contribution from the consistently regularized two-body charge density \hat{O}_{2b} at next-to-next-to-next-to-leading order (N³LO), consisting of contact (Cont) and one-pion-exchange (1 π) terms, is

$$\langle M' | \hat{O}_{2b} | M \rangle = \sum_{\alpha_{12} \alpha'_{12}} \int dp_{12} \int dp'_{12} p_{12}^2 p'_{12}^2 \times \rho_{2b}^{M'M} (p'_{12}, p_{12}; \vec{q}) \hat{O}_{2b}^{M'M} (\alpha'_{12} \alpha_{12}; p'_{12}, p_{12}) \quad (S2)$$

where $\alpha \equiv (l_{12} s_{12}) j_{12} t_{12} m_{t12}$ labels the two-body partial-wave channels and the relative momentum is p_{12} [50]. Once the partial-wave decomposition is done, the resulting matrix elements of the charge operators are used for all the nuclei. The nuclear many-body information is encoded in the one- and two-body density matrices, constructed based on the J-NCSM calculations available online at [52]. The matrix elements of one- and two-charge density operator are calculated by performing a numerical partial wave decomposition based on [51].

B. Determination of isospin-1 channel LEC M_3

There are three LECs, M_1 , M_2 , and M_3 in the isoscalar two-body contact charge density operators

$$\begin{aligned} \rho_{\text{Cont}}(\mathbf{k}) = 2eG_E^S(\mathbf{k}^2) & \left[M_1 \frac{\boldsymbol{\sigma}_1 \cdot \boldsymbol{\sigma}_2 + 3}{4} \frac{1 - \boldsymbol{\tau}_1 \cdot \boldsymbol{\tau}_2}{4} \mathbf{k}^2 \right. \\ & + M_2 \frac{1 - \boldsymbol{\tau}_1 \cdot \boldsymbol{\tau}_2}{4} \left((\mathbf{k} \cdot \boldsymbol{\sigma}_1)(\mathbf{k} \cdot \boldsymbol{\sigma}_2) - \frac{1}{3}(\boldsymbol{\sigma}_1 \cdot \boldsymbol{\sigma}_2)\mathbf{k}^2 \right) \\ & \left. + M_3 \frac{1 - \boldsymbol{\sigma}_1 \cdot \boldsymbol{\sigma}_2}{4} \left(\frac{\boldsymbol{\tau}_1 \cdot \boldsymbol{\tau}_2 + 3}{4} \right) \mathbf{k}^2 \right], \end{aligned}$$

where \mathbf{k} is the photon momentum and $G_E^S(\mathbf{k}^2)$ is isoscalar nucleon charge form factor taken from [54]. The details of

the contact charge density operator and its regularization can be found in Ref. [39]. LECs M_1 , M_2 , M_3 are related to LECs A , B , C defined in [5, 39, 42] as

$$M_1 = A + B + C/3, \quad M_2 = C, \quad M_3 = A - 3B - C. \quad (S3)$$

All LECs above have units of $F_\pi^{-2} \Lambda_b^{-3}$, where $\Lambda_b = 650$ MeV refers to the breakdown scale of the chiral expansion and $F_\pi = 92.4$ MeV is the pion decay constant. The isospin-zero-to-isospin-zero channel LECs, M_1 and M_2 , can be fitted to the deuteron charge and quadrupole form factors, and have already been determined in Ref. [39]. In this work, to accurately determine the LEC M_3 in the isospin-1-to-isospin-1 channel we use the high precision charge radius of ${}^4\text{He}$ from muonic atom measurement 1.67824(83) fm [8].

The charge radius of ${}^4\text{He}$ is calculated via Eq. (2) using the one- and two-body density matrix from FY method with the bare SMS interactions. The matter radius contribution r_m is directly obtained using the two-body densities at zero momentum transfer. The contributions from the DF, SO, and two-body one-pion-exchange and contact operators are extracted by using

$$R_c^2 = -6 \frac{\partial F(q^2)}{\partial q^2} \Big|_{q^2=0}. \quad (S4)$$

In practice, the calculated FFs are fitted to the function $F(q^2) = 1 + aq^2 + bq^4 + cq^6$ in the q interval $(0, 0.5)$ fm⁻¹ and the charge radius is extracted as $R_c = \sqrt{-6a}$. We mention that the boost corrections are not included in our fitting procedure.

For the interaction SMS N⁴LO⁺ + N²LO with $\Lambda_N = 450$ MeV and $\Lambda_N = 500$ MeV, the obtained values of the LEC M_3 read $M_3 = (-2.44 \pm 0.13) F_\pi^{-2} \Lambda_b^{-3}$ and $M_3 = (-2.98 \pm 0.13) F_\pi^{-2} \Lambda_b^{-3}$, respectively.

C. Statistical uncertainties of charge radii propagated from LECs in 2N contact charge operator

Since M_3 is fitted to the experimental ${}^4\text{He}$ radius, which is known very precisely, an inverse cross-check – recomputing the ${}^4\text{He}$ radius – should reproduce an equally small uncertainty. In contrast, neglecting correlations between M_1 and M_2 for the interaction SMS N⁴LO⁺ + N²LO with cutoffs 450 MeV and 500 MeV yields uncertainties of 0.0022 fm and 0.0019 fm, respectively. These values are several times larger than the experimental precision. Nevertheless, neglecting correlations is sufficient to provide a very conservative estimate for the uncertainty propagated to heavier nuclei, as the induced errors remain significantly smaller than other sources of uncertainty.

Employing the three LECs discussed above, we examined the resulting uncertainties for the p-shell nu-

clei ${}^6\text{Li}$ and ${}^8\text{Be}$. The J-NCSM calculations were performed with $\omega_{\text{HO}} = 18.0$ MeV and $N_{\text{HO}}=14$, using the SMS interaction with $\Lambda = 450$ MeV evolved via SRG $\lambda = 2.236 \text{ fm}^{-1}$, which reproduces the binding energy of ${}^6\text{Li}$. For ${}^6\text{Li}$, we obtain for the charge radius $R_c = (2.3388 \pm 0.0016_{\text{stat.}}) \text{ fm}$, where the quoted uncertainty reflects the propagated uncertainty from the LECs. After tail correction, the charge radius is well reproduced.

A similar analysis was performed for ${}^8\text{Be}$, using the J-NCSM calculations with $\omega_{\text{HO}} = 18.0$ MeV and $N_{\text{HO}}=10$, and the SMS interaction with $\Lambda = 450$ MeV SRG-evolved to 1.88 fm^{-1} . In this case, the uncertainty induced by the LECs is only about 0.0020 fm .

In summary, the uncertainties from the LECs for p -shell nuclei are very small. Therefore, in the main text, we show the results using the central values of the three LECs.

D. Matter radius with the two-body relative density

To assess the influence of the SRG transformation on the charge radius, we calculate the proton matter radius r_m^{SRG} of ${}^6\text{Li}$ and ${}^8\text{Be}$ from the two-body relative densities in r -space. This is obtained by performing the Fourier transformation on the two-body density matrix in momentum space, following the method introduced in Ref. [60], where the SRG transformation is already accounted for by constructing the two-body transition density matrix with SRG evolved nuclear many-body wave functions from J-NCSM calculations. The matter radius is calculated using the formulas introduced in Ref. [65]. In this way, the SRG influence on charge radii is considered at the two-body level and the induced three-body part is neglected.

E. Charge form factors and radius of ${}^6\text{Li}$ and ${}^8\text{Be}$ from J-NCSM

In Figs. S1 and S2, we show the charge FFs of ${}^6\text{Li}$ using J-NCSM with the chiral interaction SMS $\text{N}^4\text{LO}^+ + \text{N}^2\text{LO}$ $\Lambda_N = 450$ MeV evolved to flow parameters 1.88, 2.236 and 2.600 fm^{-1} . We show the results with two ω_{HO} values, 18.0 and 20.0 MeV, and $N_{\text{HO}} = 6, 8, 10, 12$, and 14 and when $N_{\text{HO}} = 14$, the calculated binding energies are also close to the data. Especially when increasing SRG flow parameter λ , the charge FFs in medium momentum transfers, $(2.0, 2.8) \text{ fm}^{-1}$, are closer to data. Overall, with the increase of basis size N_{HO} and SRG flow parameter, the calculated FFs are well consistent with the measurements, and the two-body charge contribution plays an important role for high momentum transfers. Thereby, the effects from HO basis size and frequency are non-significant.

In Fig. S3, we show the contribution $\Delta R_{\text{Cont}+1\pi}$ from the contact and one-pion-exchange operators to the charge radius of ${}^6\text{Li}$ with different J-NCSM basis frequencies and model spaces and for different SRG flow parameters. It can be seen that $\Delta R_{\text{Cont}+1\pi}$ is converged with respect to N_{HO} up to approximately 0.001 fm especially when considering $\omega_{\text{HO}} = 16$ and 18 MeV, which are optimal for the convergence of the binding energy.

For ${}^8\text{Be}$, similar calculations have also been performed. In Fig. S4, we show the charge FFs for four ω_{HO} values using the interaction SMS $\text{N}^4\text{LO}^+ + \text{N}^2\text{LO}$ $\Lambda_N = 450$ MeV evolved to flow parameter 1.88 fm^{-1} . Due to the limited basis size in J-NCSM, the maximum HO model space is 10. For the optimal HO frequencies 16.0 and 18.0 MeV, the differences in FFs are insignificant. In Fig. S5, we show the contribution of OPE and contact term on charge radius, $\Delta R_{\text{Cont}+1\pi}$, as a function of N_{HO} for different ω_{HO} and we find that for $\omega_{\text{HO}} = 16$ and 18 MeV, $\Delta R_{\text{Cont}+1\pi}$ are almost converged and the value is about 0.034 fm.

Calculations with J-NCSM using the interaction SMS $\text{N}^4\text{LO}^+ + \text{N}^2\text{LO}$ for $\Lambda_N = 500$ MeV yield conclusions for the effects of 2N charge operators on ${}^6\text{Li}$ and ${}^8\text{Be}$ that are almost the same as for $\Lambda = 450$ MeV.

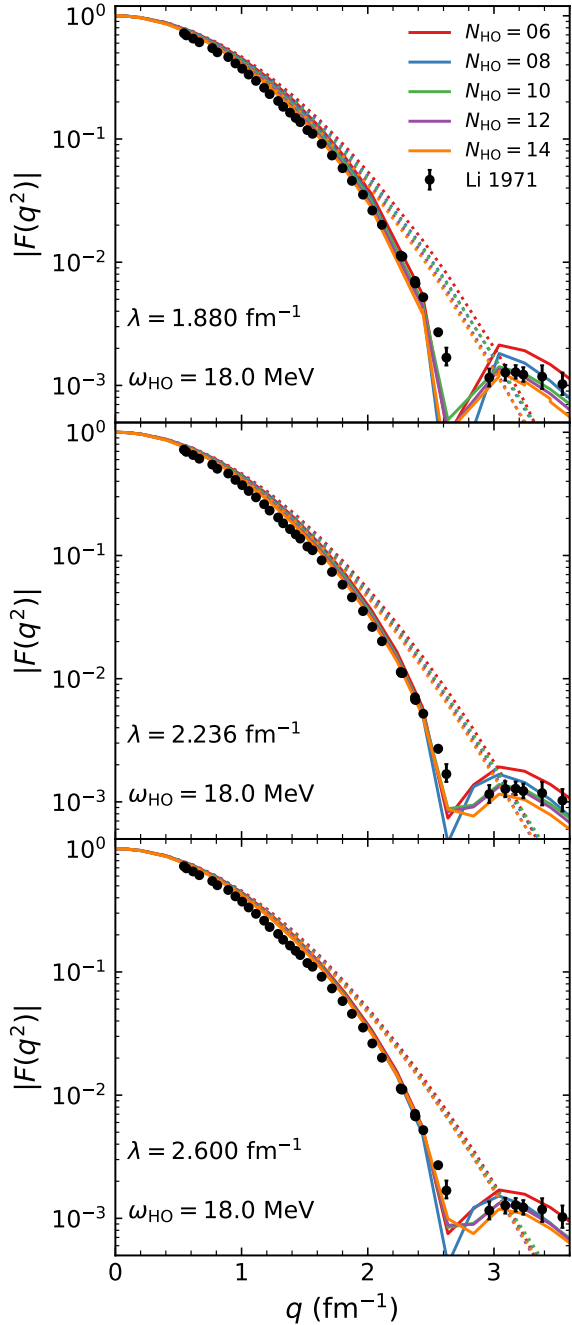


FIG. S1. Charge form factor of ${}^6\text{Li}$ from J-NCSM calculations with $\omega = 18.0$ MeV and different N_{HO} . The adopted interaction is SMS $\text{N}^4\text{LO}^+ + \text{N}^2\text{LO } \Lambda_N = 450$ MeV evolved to flow parameters 1.88 , 2.236 and 2.600 fm^{-1} . The dotted lines present the results with one-body operators and solid lines for cases considering the 2N operators. Experimental data are taken from Ref. [59].

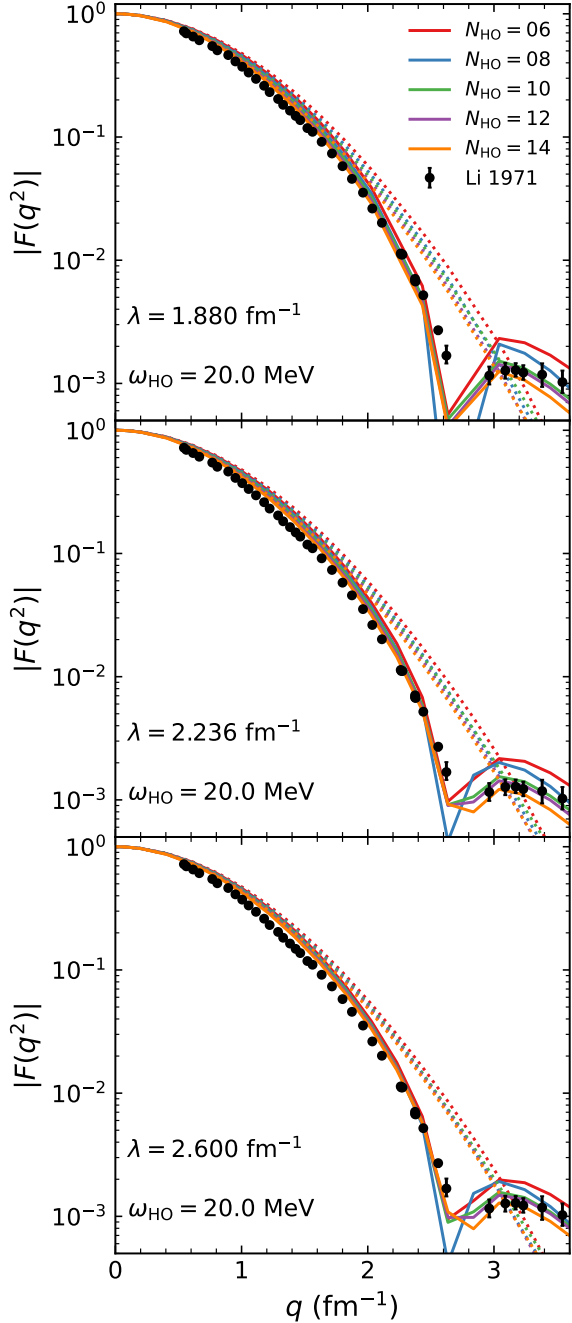


FIG. S2. Charge form factor of ${}^6\text{Li}$ from J-NCSM calculations with $\omega = 20.0$ MeV and different N_{HO} . The adopted interaction is SMS $\text{N}^4\text{LO}^+ + \text{N}^2\text{LO } \Lambda_N = 450$ MeV evolved to flow parameter 1.88 , 2.236 , and 2.600 fm^{-1} . The dotted lines represent the results with one-body operators and solid lines for cases considering the 2N operators. Experimental data are taken from Ref. [59].

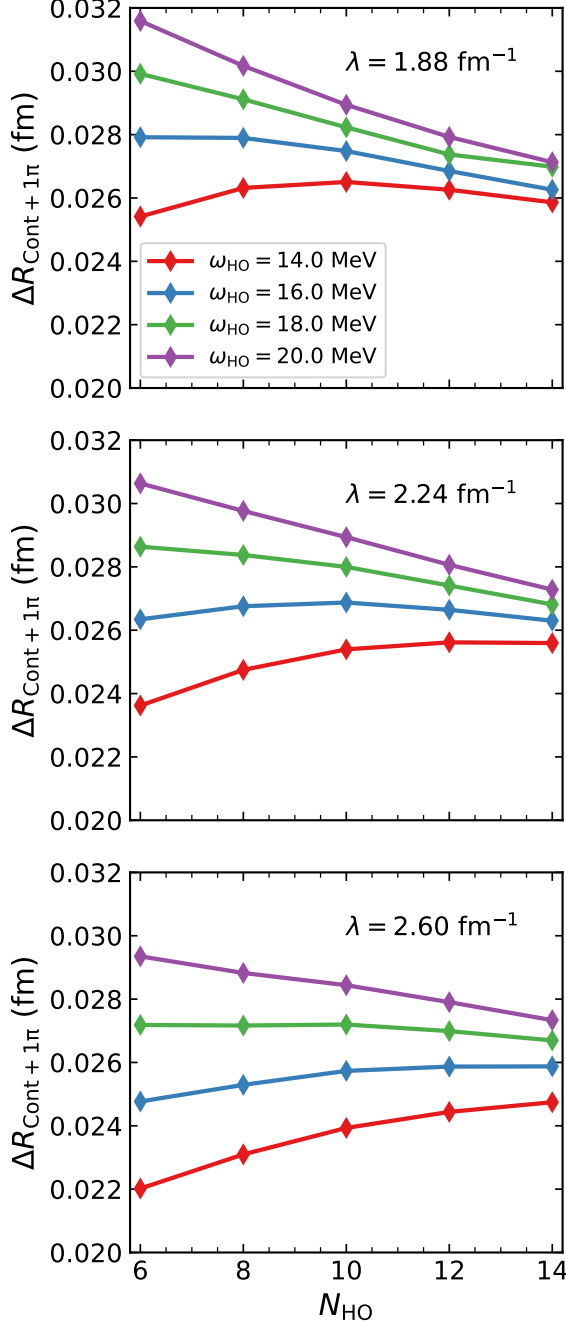


FIG. S3. Contribution from two-nucleon contact and one-pion-exchange terms to the charge radii of ${}^6\text{Li}$ from J-NCSM calculations with different HO parameters. The adopted interaction is SMS $\text{N}^4\text{LO}^+ + \text{N}^2\text{LO}$ $\Lambda_N = 450 \text{ MeV}$ evolved to flow parameter $1.88, 2.236$ and 2.600 fm^{-1} .

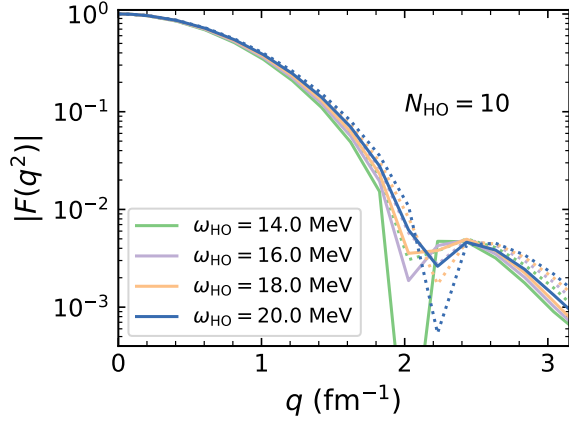


FIG. S4. Charge form factor of ${}^8\text{Be}$ from J-NCSM calculations with $N_{\text{HO}}=10$ and different ω . The adopted interaction is SMS $\text{N}^4\text{LO}^+ + \text{N}^2\text{LO } \Lambda_N = 450 \text{ MeV}$ evolved to flow parameter 1.88 fm^{-1} . The dashed lines indicate the results using 1N operators and the solid lines are those including 2N operator contributions.

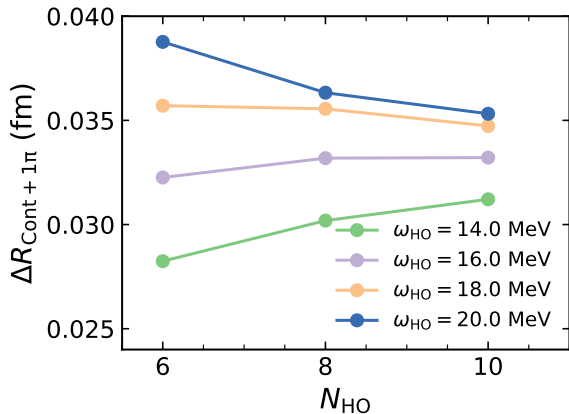


FIG. S5. Contribution from two-nucleon contact and one-pion-exchange terms to the charge radii of ${}^8\text{Be}$ from J-NCSM calculations with different HO parameters. The adopted interaction is SMS $\text{N}^4\text{LO}^+ + \text{N}^2\text{LO } \Lambda_N = 450 \text{ MeV}$ evolved to flow parameter 1.88 fm^{-1} .